



Fast and robust reconstruction algorithm for fluorescence diffuse optical tomography assuming a cuboid target

CHUNLONG SUN,^{1,2} GEN NAKAMURA,² GORO NISHIMURA,³ YU JIANG,⁴ JIJUN LIU,¹ AND MANABU MACHIDA^{5,*}

¹School of Mathematics, Southeast University, Nanjing 210096, China

²Department of Mathematics, Hokkaido University, Sapporo 060-0810, Japan

³Research Institute for Electronic Science, Hokkaido University, Sapporo 001-0020, Japan

⁴School of Mathematics, Shanghai University of Finance and Economics, Shanghai 200433, China

⁵Institute for Medical Photonics Research, Hamamatsu University School of Medicine, Hamamatsu 431-3192, Japan

*Corresponding author: machida@hama-med.ac.jp

Received 16 September 2019; revised 4 December 2019; accepted 4 December 2019; posted 4 December 2019 (Doc. ID 377152); published 10 January 2020

A fast algorithm for fluorescence diffuse optical tomography is proposed. The algorithm is robust against the choice of initial guesses. We estimate the position of a fluorescent target by assuming a cuboid (rectangular parallelepiped) for the fluorophore target. The proposed numerical algorithm is verified by a numerical experiment and an experiment with a meat phantom. The target position is reconstructed with a cuboid from measurements in the time domain. Moreover, the long-time behavior of the emission light is investigated making use of the analytical solution to the diffusion equation. © 2020 Optical Society of America

<https://doi.org/10.1364/JOSAA.37.000231>

1. INTRODUCTION

Fluorescence diffuse optical tomography (FDOT) is one type of optical tomography that makes use of fluorescent light from fluorophore. In FDOT, diffuse light from fluorophore, such as indocyanine green (ICG), is detected on the boundary of biological tissue to obtain tomographic images [1,2]. FDOT can be formulated as an inverse source problem. As theoretical results, in addition to the usual L^2 regularization, the L^1 regularization was tested [3–6], and the total variation was considered [7]. An improvement in image quality was reported with the total variation by making use of the Bregman distance [8]. In data acquisition, the measured fluorescent light can be divided by the measured excitation light to cancel unknown constants, which was introduced as normalized measurements [9].

FDOT has been verified *in vivo* [10,11] and also in clinical research for breast cancer [12–14]. Noncontact measurements with a CCD camera were established, and fluorescence yield was reconstructed for mice with lung tumors [15]. The resolution of tomographic images is a function of the number of sources and detectors. A large number of parallel channels can be employed by a detection fiber array coupling onto a CCD camera, which leads to fluorescence molecular tomography finding a target of a few millimeters [16,17]. A tumor in a mouse was imaged by the use of a conical mirror, by which light is collected by a CCD

camera without attaching optical fibers to the mouse [18]. As an alternative, the number of measured data can be increased by time-dependent experiments [19]. The superiority of the time-resolved approach over the continuous-wave approach in FDOT was concluded [20], although the quality of images can be improved even for a time-independent experiment if a large data set is used [21]. In FDOT, usually it is not easy to know precise values of absorption and scattering coefficients. The reduction in the reconstruction errors due to this inaccuracy is proposed with the Bayesian approximation error approach [22].

Among three types of FDOT (continuous wave, frequency domain, and time domain), the measurement in time domain has the most fruitful information. Although the governing equation for near-infrared light in the frequency domain reduces to the time-independent diffusion equation, the time-resolved curve for the time-domain FDOT is calculated from the time-dependent diffusion equation. Usually, the information carried by measurements in time domain is not fully explored. By a transformation in time such as Fourier transform, Laplace transform, Mellin transform, Mellin–Laplace transform, etc., the problem is reduced to an inverse problem for the time-independent diffusion equation [23].

A straightforward way of solving the linear inverse problem of FDOT is the direct inversion with singular value decomposition (SVD). Although SVD is proven to be successful [21],

the method is computationally expensive from the viewpoint of memory and speed. An alternative approach is the use of iterative methods. For example, the Levenberg–Marquardt (LM) method [24,25] has been successfully used for FDOT of breast cancer in the frequency domain [12]. By the regularization of total variation, edges in reconstructed images are not smoothed. However, compared with the usual L^2 regularization, some care is necessary for the use of total variation. To this end, the split Bregman iteration was developed [26,27] and used in Ref. [7]. The three-dimensional FDOT in the time domain with the time-dependent diffusion equation is still a challenging problem. In Ref. [19], reconstructed images for the time-domain FDOT by the time-dependent diffusion equation were obtained in two dimensions by an iterative scheme of the Newton–Raphson inversion. Two-dimensional time-dependent diffusion equations were solved for the FDOT by the total light approach [28,29]. Although the original coupled diffusion equations are simplified by this approach, the corresponding inverse problem becomes more difficult, since the approach makes use of the weak nonlinearity of the FDOT inverse problem, which is almost linear.

In this paper, we consider FDOT by measuring time-resolved data from reflected light. Aiming at a fast and robust numerical algorithm, we focus on the reconstruction of the position of a fluorophore target, neglecting its precise shape. We assume a cuboid or rectangular parallelepiped in the medium. Then we try to find the cuboid that represents the true target. Due to the assumption of the cuboid shape, the reconstruction of our FDOT can be done by determining only several unknown parameters. For the robustness and fast convergence of our reconstruction scheme, we narrow the region of interest during the reconstruction process. Before assuming a cuboid, we use a cubic to have a good initial guess. The initial guess for the cubic is chosen using the spatial knowledge of the intensity from boundary measurements. The proposed reconstruction scheme was tested both numerically and experimentally. We will consider the three-dimensional FDOT using the time-dependent diffusion equation, which is the most computationally expensive FDOT. Using the proposed method, we show that the three-dimensional FDOT in the time domain is feasible on a laptop computer (Apple MacBook Pro, 2.7 GHz Intel Core i5). If we consider continuous-wave or frequency-domain measurements, two numerical integrals are removed in our formulation [see U_m in Eq. (13)] and the computational time will be further reduced. Furthermore, we study the asymptotic behavior of the temporal profile of the emission light using the diffusion equation.

The paper is organized as follows. In Section 2, we develop the formulation of our FDOT and give an analytical formula for the emission light. The proposed numerical scheme is described in Section 3 with a numerical example of an ellipsoidal target. In Section 4, we validate our numerical method with a beef sample in which a fluorescent target is embedded. The detected emission light carries information on the target to be reconstructed. In Section 5, we study the time dependence of the emission light for a point fluorophore. Finally, Section 6 is devoted to conclusions.

2. FORMULATION

Let us suppose that a fluorescent target is embedded in biological tissue occupying the half space ($-\infty < x < \infty, -\infty < y < \infty, 0 < z < \infty$). Let c be the speed of light in the medium. Let $u_e(\mathbf{r}, t)$, $u_m(\mathbf{r}, t)$ be the energy densities of the excitation light and emission light, respectively. Here, $\mathbf{r} = (\rho, z)$, with $\rho = (x, y)$ as the position and t as time. Boundary measurements are performed during $0 < t < T$. We assume that the reduced scattering coefficient μ'_s and the absorption coefficient μ_a are constants everywhere in the medium. Although the wavelength of the emission light is longer than the wavelength of the excitation light, and thus values of μ_a and μ'_s are different for the excitation light and emission light, we ignore this difference. Moreover, compared with μ_a , the absorption coefficient for the fluorophore is negligible because it is nonzero only at the position of the fluorophore. Then in the medium ($z > 0$), $u_e(\mathbf{r}, t)$ and $u_m(\mathbf{r}, t)$ obey the following diffusion equations (e.g., [19,20]):

$$\left(\frac{1}{c} \frac{\partial}{\partial t} - D\Delta + \mu_a \right) u_e = 0, \quad (1)$$

$$\left(\frac{1}{c} \frac{\partial}{\partial t} - D\Delta + \mu_a \right) u_m = F, \quad (2)$$

where $D = 1/(3\mu'_s)$, and

$$F(\mathbf{r}, t) = \frac{n(\mathbf{r})}{\tau} \int_0^t e^{-(t-s)/\tau} u_e(\mathbf{r}, s) ds. \quad (3)$$

Here, $n(\mathbf{r})$ is proportional to the fluorophore concentration, whose proportionality constant is the product of the quantum yield and absorption cross section, and τ is the fluorescence lifetime. We assume that $u_e = 0$ and $u_m = 0$ at $t = 0$. The sample is illuminated at position $\mathbf{r}_s = (\rho_s, 0)$ by a pencil beam of the temporal profile $h(t)$ ($t > 0$) in the $x-y$ plane. At $z = 0$, u_e , u_m satisfy the Robin boundary conditions as

$$-\frac{\partial}{\partial z} u_e + \beta u_e = h(t)\delta(\rho - \rho_s), \quad -\frac{\partial}{\partial z} u_m + \beta u_m = 0. \quad (4)$$

The parameter β is given by $\beta = \frac{1}{2D}(1 - 2 \int_0^1 \mathcal{R}(\mu) \mu d\mu)/(1 + \int_0^1 \mathcal{R}(\mu) \mu^2 d\mu)$ with the Fresnel reflectance $\mathcal{R}(\mu)$, which depends on the refractive index of the medium [30]. Suppose the out-going light is detected at \mathbf{r}_d on the boundary. The excitation light and emission light are detected through a response function R as

$$U_e(\mathbf{r}_d, t; \mathbf{r}_s) = \int_0^t R(t-s) u_e(\mathbf{r}_d, s) ds, \\ U_m(\mathbf{r}_d, t; \mathbf{r}_s) = \int_0^t R(t-s) u_m(\mathbf{r}_d, s) ds, \quad (5)$$

where the function R is determined by the detector. These U_e , U_m correspond to experimentally measured light $U_e^{\text{exp}}(\mathbf{r}_d, t; \mathbf{r}_s)$, $U_m^{\text{exp}}(\mathbf{r}_d, t; \mathbf{r}_s)$.

Let $G(\mathbf{r}, \mathbf{r}'; t)$ be the Green's function that satisfies

$$\left(\frac{1}{c} \frac{\partial}{\partial t} - D\Delta + \mu_a \right) G(\mathbf{r}, \mathbf{r}'; t) = \delta(\mathbf{r} - \mathbf{r}')\delta(t), \quad (6)$$

with the initial condition $G = 0$ at $t = 0$ and the Robin boundary condition $-\frac{\partial}{\partial z}G + \beta G = 0$. The Green's function is obtained as [31–34]

$$\begin{aligned} G(\mathbf{r}, \mathbf{r}'; t) &= c(4\pi Dct)^{-3/2} e^{-\mu_a ct} \\ &\times \exp\left(-\frac{(x-x')^2 + (y-y')^2}{4Dct}\right) g(z, z'; t), \end{aligned} \quad (7)$$

where

$$\begin{aligned} g(z, z'; t) &= \\ &\exp\left(-\frac{(z+z')^2}{4Dct}\right) + \exp\left(-\frac{(z-z')^2}{4Dct}\right) - 2\beta\sqrt{\pi Dct} \\ &\times \exp(\beta(z+z') + \beta^2 Dct) \operatorname{erfc}\left(\frac{z+z' + 2\beta Dct}{\sqrt{4Dct}}\right). \end{aligned} \quad (8)$$

We introduce the instrument response function as

$$q(t) = \int_0^t R(t-s) h(s) ds. \quad (9)$$

The fluorophore target that we try to reconstruct may have different shapes. In this paper, we focus on the position of the target and solve the inverse problem assuming a cuboid. That is, we will find the location of the target using a cuboid. In the formulation below, we assume that the target has the shape of a cuboid.

Let Ω_c be a cuboid specified by $x_1, x_2, y_1, y_2, z_1, z_2$ as $x_1 < x < x_2, y_1 < y < y_2, z_1 < z < z_2$. We assume that

$$n(\mathbf{r}) = \begin{cases} M, & \mathbf{r} \in \Omega_c, \\ 0, & \mathbf{r} \notin \Omega_c, \end{cases} \quad (10)$$

where $M > 0$ is a constant. Then we obtain

$$\begin{aligned} U_m(\mathbf{r}_d, t; \mathbf{r}_s) &= \int_0^t Q(s) \int_0^{t-s} \int_{\Omega_c} n(\mathbf{r}') G(\mathbf{r}_d, \mathbf{r}'; t-s-s') \\ &\times G(\mathbf{r}', \mathbf{r}_s; s') d\mathbf{r}' ds' ds, \end{aligned} \quad (11)$$

where we introduce

$$Q(t) = \frac{D}{\tau} \int_0^t e^{-t'/\tau} q(t-t') dt'. \quad (12)$$

Equation (11) can be rewritten as

$$\begin{aligned} U_m(\mathbf{r}_d, t; \mathbf{r}_s) &= \\ &M \int_0^t Q(s) \int_0^{t-s} f_1(\rho_d, \rho_s, t-s, t'; x_1, x_2, y_1, y_2) \\ &\times f_2(t-s, t'; z_1, z_2) dt' ds, \end{aligned} \quad (13)$$

where

$$\begin{aligned} f_1(\rho_d, \rho_s, t, s; x_1, x_2, y_1, y_2) &= \\ &\frac{e^{-\mu_a ct}}{4^3 \pi^2 D^2 t \sqrt{(t-s)s}} e^{-\frac{(x_d-x_s)^2 + (y_d-y_s)^2}{4Dct}} \\ &\times [f_3(x_d, x_s, t, s; x_2) - f_3(x_d, x_s, t, s; x_1)] \\ &\times [f_3(y_d, y_s, t, s; y_2) - f_3(y_d, y_s, t, s; y_1)], \end{aligned} \quad (14)$$

and

$$f_2(t, s; z_1, z_2) = \int_{z_1}^{z_2} g(0, z'; t-s) g(z', 0; s) dz'. \quad (15)$$

Here, we define

$$\begin{aligned} f_3(x_d, x_s, t, s; x) &= \\ &\operatorname{erf}\left(\sqrt{\frac{t}{4Dc(t-s)s}} \left(x - \frac{s x_d + (t-s)x_s}{t}\right)\right). \end{aligned} \quad (16)$$

We can compute $U_m(\mathbf{r}_d, t; \mathbf{r}_s)$ using (13).

3. IDENTIFICATION OF A CUBOID

The reconstruction of a fluorophore, which in general has different shapes, is considered. In our proposed inversion scheme, we will reconstruct the fluorophore by identifying a cuboid $n(\mathbf{r})$. The cuboid is expected to specify the location of the fluorophore. In this way, our FDOT is achieved by using only seven unknown parameters: $M, x_1, x_2, y_1, y_2, z_1, z_2$. Although the number of unknown parameters is significantly fewer than other methods that use voxels, the original linear inverse problem of reconstructing $n(\mathbf{r})$ from U_m in (11) becomes nonlinear. The reconstruction will be done with the LM method. Even though there are only seven parameters, the choice of initial guesses is important. For the sake of robust reconstruction, we propose to obtain a set of good initial guesses for the seven parameters by narrowing the region of interest according to three steps described below.

Let N_{SD} be the number of source-detector pairs. The positions of each source and detector are denoted by $\mathbf{r}_s^i, \mathbf{r}_d^i$ ($i = 1, \dots, N_{SD}$). At each detector, light is measured at N_t temporal points.

We first look for a rough location of the target projected to the $x-y$ plane or a region of interest Γ on the boundary, under which the target is likely to be embedded, by observing

$$I_i = \int_0^T U_m^{\text{exp}}(\mathbf{r}_d^i, t; \mathbf{r}_s^i) dt, \quad i = 1, \dots, N_{SD}. \quad (17)$$

The observation time $T = 3$ ns for the numerical experiment in this section and $T = 10$ ns for the meat phantom experiment in Section 4. We call this step of setting Γ the topography process. By using I_i with large values, we set the region Γ .

Then we assume a cubic target whose location and size are determined by four parameters x_0, y_0, z_0, l , such that

$$\begin{aligned}x_1 &= x_0 - \frac{l}{2}, & x_2 &= x_0 + \frac{l}{2}, & y_1 &= y_0 - \frac{l}{2}, & y_2 &= y_0 + \frac{l}{2}, \\z_1 &= z_0 - \frac{l}{2}, & z_2 &= z_0 + \frac{l}{2}.\end{aligned}\quad (18)$$

Choosing the initial guess for x_0, y_0 inside Γ , we solve the inverse problem of determining x_0, y_0, z_0, l, M by the LM method. We note that the choice of M is not strict compared with other parameters. The obtained cubic is denoted by

$$\mathbf{a}_*^{\text{cubic}} = (x'_0, y'_0, z'_0, l', M'). \quad (19)$$

We refer to this step as the cubic tomography. Since we have only five parameters instead of seven, there is a good stability for the inverse problem in this step.

Finally, with the obtained values $\mathbf{a}_*^{\text{cubic}}$ as the initial guess $\mathbf{a}_0^{\text{cuboid}}$, we solve the inverse problem of determining a cuboid target. In this way, we can identify Ω_c for $n(\mathbf{r})$ by obtaining reconstructed values:

$$\mathbf{a}_*^{\text{cuboid}} = (x_1^*, x_2^*, y_1^*, y_2^*, z_1^*, z_2^*, M^*). \quad (20)$$

This last step is called the cuboid tomography. The algorithm is summarized as follows.

Step 1. (Topography process) Find Γ on the boundary.

Step 2. (Cubic tomography) By searching underneath Γ , obtain reconstructed values $\mathbf{a}_*^{\text{cubic}}$.

Step 3. (Cuboid tomography) Find $\mathbf{a}_*^{\text{cuboid}}$, starting with $\mathbf{a}_*^{\text{cubic}}$.

Below, we will demonstrate our algorithm with a numerical experiment. We set $\tau = 0$, $h(t) = R(t) = \delta(t)$. Let us set an ellipsoidal target as

$$\{x^2/1.5^2 + y^2/3^2 + (z - 11)^2/1.5^2 \leq 1\}, \quad (21)$$

where the unit of length is mm, with $n(\mathbf{r}) = 0.02 \text{ mm}^{-1}$. In the numerical experiment, 5% noise is added, and

$$U_m^{\text{exp}} = U_m(1 + 0.05\varepsilon), \quad (22)$$

where ε is drawn from the standard Gaussian distribution. We use the following $N_{\text{SD}} = 32$ source-detector pairs $p_i = (\mathbf{r}_d^i; \mathbf{r}_s^i)$ ($i = 1, \dots, N_{\text{SD}}$) on the boundary:

$$\begin{aligned}p_{4j-3} &= (\xi_j, \zeta_j + 10\sqrt{3}; \xi_j - 10, \zeta_j), \\p_{4j-2} &= (\xi_j, \zeta_j + 10\sqrt{3}; \xi_j + 10, \zeta_j), \\p_{4j-1} &= (\xi_j, \zeta_j - 10\sqrt{3}; \xi_j - 10, \zeta_j), \\p_{4j} &= (\xi_j, \zeta_j - 10\sqrt{3}; \xi_j + 10, \zeta_j)\end{aligned}\quad (23)$$

for $j = 1, \dots, 8$. Here, $(\xi_1, \zeta_1) = (-10, 10)$, $(\xi_2, \zeta_2) = (-10, 0)$, $(\xi_3, \zeta_3) = (-10, -10)$, $(\xi_4, \zeta_4) = (0, -10)$, $(\xi_5, \zeta_5) = (10, -10)$, $(\xi_6, \zeta_6) = (10, 0)$, $(\xi_7, \zeta_7) = (10, 10)$, and $(\xi_8, \zeta_8) = (0, 10)$. We set $N_t = 20$ and

$$t_k^i = t_p^i + (k - 10)\Delta t \quad (k = 1, \dots, N_t), \quad (24)$$

where $\Delta t = 6.67 \text{ ps}$, and t_p^i is the peak time of $U_m^{\text{exp}}(\mathbf{r}_d^i, t; \mathbf{r}_s^i)$ ($i = 1, \dots, N_{\text{SD}}$). Thus, we have $N_{\text{SD}} N_t (= 640)$ measured values $U_m^{\text{exp}}(\mathbf{r}_d^i, t_k^i; \mathbf{r}_s^i)$ ($i = 1, \dots, N_{\text{SD}}, k = 1, \dots, N_t$). Let \mathbf{a} be a vector that contains unknown parameters to be reconstructed. We find $\mathbf{a} = \mathbf{a}_*$ by fitting U_m to U_m^{exp} using the LM method implemented on MATLAB [35,36].

(Step 1) We find $I_4 = I_{10} = I_{17} = I_{27} = 5.9 \times 10^{-7}$, whereas $I_1 = I_{11} = I_{20} = I_{26} = 1.0 \times 10^{-9}$. Hence, we can set

$$\Gamma = \{-10 < x_0 < 10, -10 < y_0 < 10\}. \quad (25)$$

At this moment, we have no knowledge about the depth at which the target is embedded. We suppose $0 < z_0 < 30$ together with $0 < l < \min(20, 2z_0)$ and $0 < M < 10$.

(Step 2) We set the initial values of x_0, y_0 in Γ . For example, we can start from $\mathbf{a}_0^{\text{cubic}} = (x_0, y_0, z_0, l, M) = (2, 2, 5, 4, 0.1)$. The reconstructed values are

$$\mathbf{a}_*^{\text{cubic}} = (x'_0, y'_0, z'_0, l', M') = (0.0, 0.0, 11.24, 4.089, 0.0086). \quad (26)$$

We note that choosing x_0, y_0 in Γ is important for fast convergence. If we pick a point outside Γ and set $(x_0, y_0) = (-15, -15)$, more than 100 iterations are needed, whereas about 10 iterations are sufficient for $x_0, y_0 \in \Gamma$.

(Step 3) Now we give the initial guess $\mathbf{a}_0^{\text{cuboid}}$ from $\mathbf{a}_*^{\text{cubic}}$ as

$$\begin{aligned}\mathbf{a}_0^{\text{cuboid}} &= (x_1, x_2, y_1, y_2, z_1, z_2, M) \\&= \left(x'_0 - \frac{l'}{2}, x'_0 + \frac{l'}{2}, y'_0 - \frac{l'}{2}, y'_0 + \frac{l'}{2},\right. \\&\quad \left.z'_0 - \frac{l'}{2}, z'_0 + \frac{l'}{2}, M'\right).\end{aligned}\quad (27)$$

Then assuming that the target is a cuboid, we obtain reconstructed values $\mathbf{a}_*^{\text{cuboid}}$ as

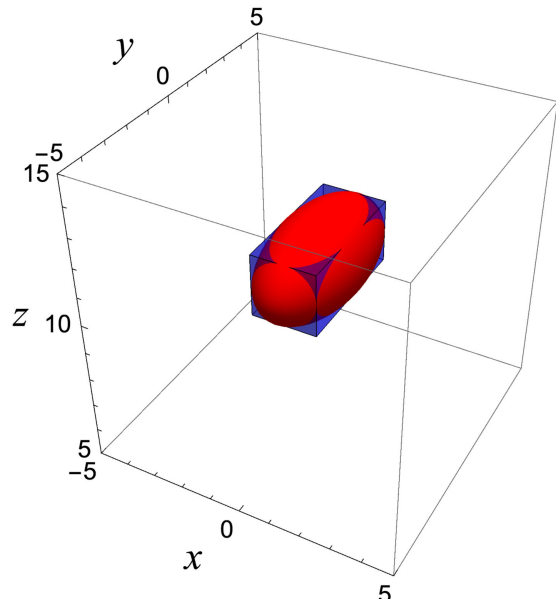


Fig. 1. Identification of the ellipsoidal target by a cuboid. The obtained cuboid given by $\mathbf{a}_*^{\text{cuboid}}$ (blue) is shown with the ellipsoid (red).

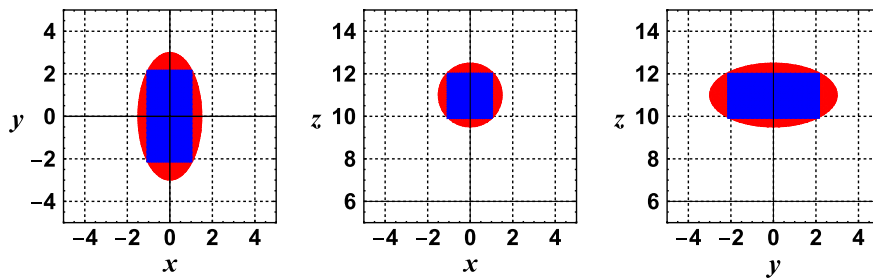


Fig. 2. Same as Fig. 1 but cross sections are shown. The cuboid (blue) and ellipsoid (red) are shown, from the left, on the plane at $z = 11$, on the $x-z$ plane, and on the $y-z$ plane, respectively.

$$\begin{aligned} \mathbf{a}_*^{\text{cuboid}} &= (x_1^*, x_2^*, y_1^*, y_2^*, z_1^*, z_2^*, M^*) \\ &= (-1.074, 1.036, -2.146, 2.166, 9.908, 12.02, 0.029). \end{aligned} \quad (28)$$

The reconstructed cuboid is shown in Fig. 1 with the ellipsoidal target. The cuboid (blue) and ellipsoid (red) are shown in two-dimensional planes in Fig. 2. We see that the center position of the ellipsoidal target is correctly reconstructed, and the volume of the target is well recovered by the cuboid. Furthermore, the reconstructed M^* is close to the true value 0.02 mm^{-3} .

Figure 2 shows that the reconstructed cuboid is the one that has the largest area in the ellipse on each projected plane: $x-y$, $x-z$, or $y-z$. In the $x-y$ plane, the cross section of the target is an ellipse of area $\pi(1.5)(3) \approx 14.1$. From the inequality $\sqrt{(x^2/1.5^2)(y^2/3^2)} \leq \frac{1}{2}(x^2/1.5^2 + y^2/3^2) = \frac{1}{2}$, we see that

$$\begin{aligned} p_1 &= (-5 - 10\sqrt{3}, 0; -5, 10), \quad p_2 = (-5 + 10\sqrt{3}, 0; -5, 10), \quad p_3 = (-5 - 10\sqrt{3}, 5; -5, 15), \quad p_4 = (-5 + 10\sqrt{3}, 5; -5, 15), \\ p_5 &= (-10\sqrt{3}, 0; 0, 10), \quad p_6 = (-10\sqrt{3}, 5; 0, 15), \quad p_7 = (5 - 10\sqrt{3}, 5; 5, -5), \quad p_8 = (5 - 10\sqrt{3}, 5; 5, 15), \\ p_9 &= (5 - 10\sqrt{3}, 0; 5, 10), \quad p_{10} = (5 - 10\sqrt{3}, -5; 5, 5), \quad p_{11} = (-10\sqrt{3}, -5; 0, 5), \quad p_{12} = (-10 + 10\sqrt{3}, 0; -10, 10), \\ p_{13} &= (-15 + 10\sqrt{3}, 0; -15, 10), \quad p_{14} = (-15 + 10\sqrt{3}, 5; -15, -5), \quad p_{15} = (-15 + 10\sqrt{3}, 5; -15, 15), \\ p_{16} &= (-10 + 10\sqrt{3}, 5; -10, 15), \end{aligned} \quad (29)$$

the maximum area of the rectangle inside the ellipse is nine, since the area is $(2x)(2y) \leq 4(1.5 \times 3)/2 = 9$. The area of the cross section of the reconstructed cuboid (Fig. 2 (Left)) is $(x_2^* - x_1^*)(y_1^* - y_2^*) = 9.098$. Similarly, in the $x-z$ plane [Fig. 2 (middle)] and $y-z$ plane [Fig. 2 (right)], the cross sections of the cuboid have the largest areas in the corresponding ellipses.

We emphasize that the narrowing process $\Gamma \rightarrow \mathbf{a}_0^{\text{cubic}} \rightarrow \mathbf{a}_0^{\text{cuboid}}$ is essential. If the initial guess $\mathbf{a}_0^{\text{cubic}}$ for step 2 is used as the initial guess for the cuboid tomography, the iteration of the LM method does not converge except for some special cases.

4. BEEF EXPERIMENT

Let us reconstruct a fluorescent tube embedded in beef with our reconstruction scheme. The tube contains $1 \mu\text{M}$ ICG solution.

Figure 3 shows how the tube is placed in the meat phantom. The tube has the shape of a cylinder of length 8 mm and diameter 2 mm. Time-dependent measurements were conducted using a holder placed on the top of the beef sample as shown in Fig. 3. Four optical fibers (two are for sources, and the other two are for detectors) are attached to the holder. The motorized stage on which the meat phantom is placed changes positions while the holder is fixed. A near-infrared pulsed laser at 780 nm is used to excite the fluorescent target. See [37] for the experimental setup. Since the source-detector separation is 2 cm, we can assume the half space.

Optical parameters for the meat phantom are $\mu'_s = 0.92 \text{ mm}^{-1}$, $\mu_a = 0.023 \text{ mm}^{-1}$. The refractive index is set to 1.37. Moreover, $\tau = 0.6 \text{ ns}$ [38]. By neglecting source-detector pairs with tiny signals, we can use $N_{SD} = 16$ source-detector pairs $p_i = (\mathbf{r}_s^i; \mathbf{r}_d^i)$ ($i = 1, \dots, N_{SD}$):

where the unit of coordinates is mm. The background fluorescence is subtracted from the signal at each source-detector pair. Since the signal from the source-detector pair $p_0 = (-15 - 10\sqrt{3}, 5; -15, 15)$ contains little contribution from the target fluorescence, we used the emission light from p_0 as the background fluorescence. Sources and detectors are shown in Fig. 4. Red small disks show sources and blue circles show detectors. The source-detector pairs are denoted by pink lines. Moreover, the green rectangle shows the position of the reconstructed tube in (32) projected on the $x-y$ plane. We set $N_t = 20$ and $\Delta t = 6.1 \text{ ps}$. At the i th source-detector pair ($i = 1, \dots, N_{SD}$), measured times used for reconstruction are $t_k^i = t_p^i + (k - 1)\Delta t$ ($k = 1, \dots, N_t$), where t_p^i is the peak time of $U_m^{\text{exp}}(\mathbf{r}_d^i, t; \mathbf{r}_s^i)$.

Since measured values are large in this region, such as $I_5 = 3.3 \times 10^4$, $I_6 = 4.0 \times 10^4$, $I_{12} = 2.9 \times 10^4$,

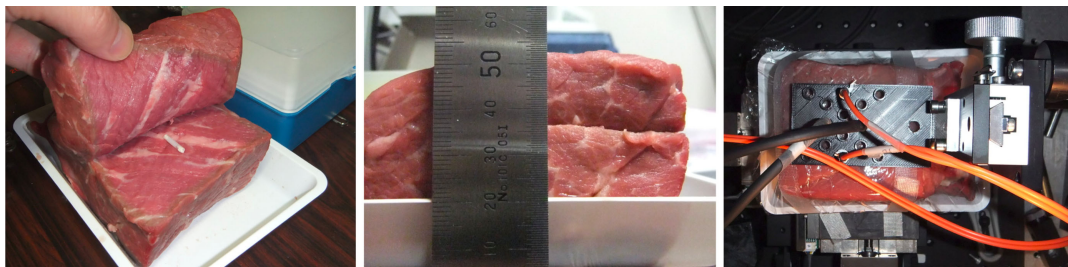


Fig. 3. (Left) A tube of ICG was placed inside the beef. (Middle) The tube was embedded at a depth of about 16 mm. (Right) Boundary measurements were performed using optical fibers attached to a holder on the top of the beef.

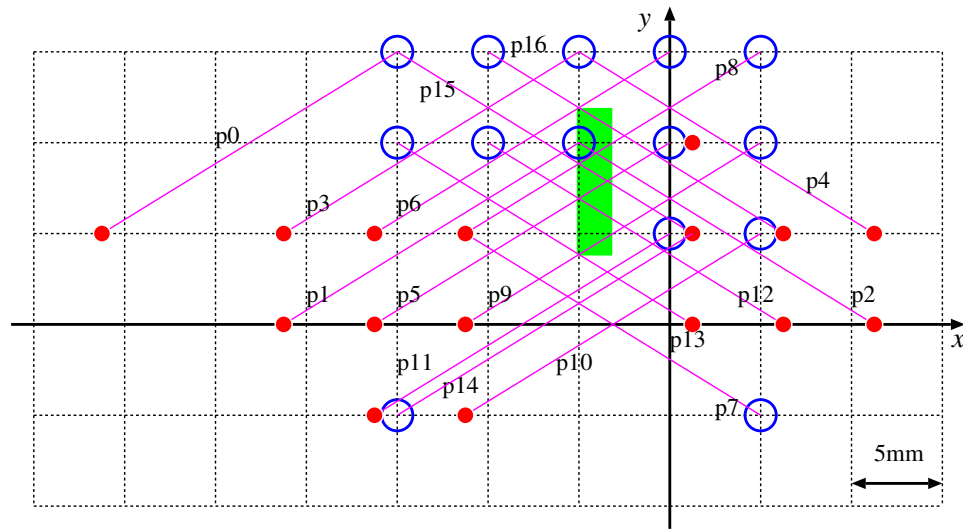


Fig. 4. Schematic figure of measurements on the boundary. Red small disks show sources, and blue circles show detectors. The source-detector pairs are denoted by pink lines. The green rectangle shows the position of the reconstructed tube projected on the x - y plane.

$$I_{16} = 3.4 \times 10^4, \text{ first we set (step 1)}$$

$$\Gamma = \{-10 < x < 0, 5 < y < 20\}. \quad (30)$$

Although the value of $n(\mathbf{r})$, i.e., M for the cube and cuboid, is a parameter to be reconstructed, in this beef experiment, M is determined only up to a constant that comes from the property of the instrument. We set $(x_0, y_0, z_0) = (-5, 10, 7)$, $l = 2$, and obtain (step 2)

$$(x'_0, y'_0, z'_0) = (-4.12, 7.72, 17.25), \quad l' = 3.92. \quad (31)$$

With the above values as the initial guess, we use the iterative method once again (step 3). The reconstructed values are obtained as

$$\begin{aligned} x_1^* &= -5.16, & x_2^* &= -3.11, & y_1^* &= 3.83, & y_2^* &= 12.03, \\ z_1^* &= 16.05, & z_2^* &= 16.34. \end{aligned} \quad (32)$$

The position of the cuboid is what we expected. In particular, we see that the orientation of the cylinder must be almost parallel to the y axis as shown in Fig. 4. Thus, the position of the fluorescent tube is reconstructed with the proposed numerical scheme.

The exact position of the embedded tube in beef is not known. If the tube is parallel to the y axis as the green rectangle in Fig. 4, the reconstructed diameter of the tube is $x_2^* - x_1^* = 2.05$ mm, and the reconstructed length of the tube is $y_2^* - y_1^* = 8.2$ mm, where the true diameter and length are 2 mm and 8 mm, respectively. The reconstructed depth position is estimated as $(z_1^* + z_2^*)/2 = 16.2$ mm, which is consistent with the depth shown in Fig. 3 (middle). Compared with these reconstructed values, the reconstructed thickness $z_2^* - z_1^* = 0.29$ mm is different from the diameter of the tube. In light of the fact that the ellipsoid is correctly reconstructed in Section 3, the reason for the short reconstructed thickness may be attributed to experimental conditions such as the number and positions of source-detector pairs and measurement noise.

5. LONG-TIME BEHAVIOR

The measured emission light U_m has information on the fluorophore target. Let us investigate the long-time behavior of U_m . We will see below that the fluorescence lifetime τ can be estimated by the long-time behavior of U_m .

For simplicity, we consider a point target

$$n(\mathbf{r}) = \delta(\mathbf{r} - \mathbf{r}_c). \quad (33)$$

That is, Ω_c is a point \mathbf{r}_c . According to (11), the emission light $U_m(\mathbf{r}_d, t; \mathbf{r}_s)$ can be calculated as

$$U_m(\mathbf{r}_d, t; \mathbf{r}_s) = \frac{1}{16(\pi D)^3 c} \int_0^t Q(t-s) e^{-\mu_a c s} \times \int_0^s \xi(s, s') e^{\xi(s, s')} ds' ds. \quad (34)$$

Here we introduced

$$\begin{aligned} \xi(s, s') &= \frac{1}{[(s - s')^2]^{3/2}} \\ &\times \left[1 - \beta \sqrt{\pi D c (s - s')} W\left(\frac{z_c + 2\beta D c (s - s')}{\sqrt{4 D c (s - s')}}\right) \right] \\ &\times \left[1 - \beta \sqrt{\pi D c s'} W\left(\frac{z_c + 2\beta D c s'}{\sqrt{4 D c s'}}\right) \right], \end{aligned} \quad (35)$$

and

$$\xi(s, s') = -\frac{|\mathbf{r}_s - \mathbf{r}_c|^2}{4 D c (s - s')} - \frac{|\mathbf{r}_d - \mathbf{r}_c|^2}{4 D c s'}, \quad (36)$$

where we write

$$\text{erfc}(x) = e^{-x^2} W(x). \quad (37)$$

We note that $W(x) \sim 1/(x\sqrt{\pi})$ for large x , and

$$\min_{t \in (0, T)} \frac{z_c + 2\beta D c t}{\sqrt{4 D c t}} = \sqrt{2\beta z_c}. \quad (38)$$

Let us suppose

$$z_c \gg \frac{1}{2\beta}. \quad (39)$$

Using the method of steepest descent, we obtain

$$U_m(\mathbf{r}_d, t; \mathbf{r}_s) \approx$$

$$\begin{aligned} &\frac{z_c^2}{8(\pi D)^{5/2} \sqrt{c}} \frac{(|\mathbf{r}_s - \mathbf{r}_c| + |\mathbf{r}_d - \mathbf{r}_c|)^3}{|\mathbf{r}_s - \mathbf{r}_c| |\mathbf{r}_d - \mathbf{r}_c|} \\ &\times \int_0^t Q(t-s) \frac{e^{-\mu_a c s}}{s^{3/2}} \exp\left(-\frac{(|\mathbf{r}_s - \mathbf{r}_c| + |\mathbf{r}_d - \mathbf{r}_c|)^2}{4 D c s}\right) \\ &\times \frac{1}{C_0 z_c + 2\beta D c |\mathbf{r}_s - \mathbf{r}_c| s} \frac{1}{C_0 z_c + 2\beta D c |\mathbf{r}_d - \mathbf{r}_c| s} ds, \end{aligned} \quad (40)$$

where $C_0 = |\mathbf{r}_s - \mathbf{r}_c| + |\mathbf{r}_d - \mathbf{r}_c|$. Below, we put $h(t) = R(t) = \delta(t)$ for simplicity.

We note that

$$Q(t) = \frac{D}{\tau} e^{-t/\tau}. \quad (41)$$

By considering large t , we assume the following relations:

$$t \gg \tau, \quad \tau \gg \frac{z_c}{2\beta D c}. \quad (42)$$

Since we are interested in the long-time behavior of $U_m(\mathbf{r}_d, t; \mathbf{r}_s)$, we take the Laplace transform for t and take only small values of the Laplace variable into account. Then for large t , we have

$$U_m(\mathbf{r}_d, t; \mathbf{r}_s) \propto \exp\left[-\frac{1}{\tau} \left(t - \frac{|\mathbf{r}_s - \mathbf{r}_c| + |\mathbf{r}_d - \mathbf{r}_c|}{2c\sqrt{\mu_a D}}\right)\right]. \quad (43)$$

Therefore, we obtain

$$\tau = \left(-\frac{\partial}{\partial t} \ln U_m(\mathbf{r}_d, t; \mathbf{r}_s)\right)^{-1}. \quad (44)$$

In Sections 3 and 4, we have developed the reconstruction algorithm using a pre-determined fluorescence lifetime, which is not always known *a priori*. Kumar *et al.* pointed out that the fluorescence lifetime can be estimated from the asymptotic behavior of the temporal profile of the emission light [39,40]. Here, we showed that their formula also holds true in the presence of the boundary.

6. CONCLUSION

By giving up the reconstruction of the detailed shape of the target, we can estimate the position of the target by reconstructing only several unknown parameters. Even for these several parameters, the LM method is not stable or converges slowly unless good initial guesses are used [41,42]. Thus, the proposed procedure of narrowing target domains as $\Gamma \rightarrow \mathbf{a}_0^{\text{cubic}} \rightarrow \mathbf{a}_0^{\text{cuboid}}$ is important for the iterative method to work.

In general, the fluorescence lifetime is also an unknown parameter. By the analysis in Section 5, we found that the lifetime can be estimated by observing the long-time behavior of $U_m(\mathbf{r}_d, t; \mathbf{r}_s)$ in the case of a point fluorophore. Kumar *et al.* obtained the formula (44) for an infinite homogeneous medium, and its validity was checked by Monte Carlo simulation [39]. This has been developed as the asymptotic time domain approach, in which resolution below the point spread function can be obtained [40,43]. In this paper, the formula (44) was derived in the presence of the boundary.

In Ref. [44], the domain is assumed to contain simply connected subdomains with constant optical parameters. In this paper, the cuboid target with constant optical parameters freely moves in the domain during the search process. The computational advantage of assuming a cuboid is that the solution U_m is obtained in a simple expression, as shown in (13).

The proposed algorithm was developed in the half-space. The ideas of assuming a simple shape for the target and of decreasing the number of unknown parameters step by step can be applied to more general cases where the diffusion equation must be numerically solved by the finite difference method or finite element method [45]. In addition, the use of the LM method is not essential; the proposed algorithm also works with other iterative schemes such as the conjugate gradient method and the damped Gauss–Newton method.

In this paper, the algorithm was formulated assuming a single target. The generalization of the method for multiple targets is straightforward, at least if the number of targets is known.

Funding. Japan Society for the Promotion of Science (15H05740, 15K21766, 17H02081, 17K05572, 18K03438, 19K04421); National Natural Science Foundation of China (11971104, 11531005, 11871149, 11971121, 91730304); Postgraduate Research & Practice Innovation Program of Jiangsu Province (KYCX18_0051).

Acknowledgment. The authors appreciate the A3 foresight program: Modeling and Computation of Applied Inverse Problems by the Japan Society for the Promotion of Science (JSPS). C. Sun is supported by the Postgraduate Research & Practice Innovation Program of Jiangsu Province, and NSFC. G. Nakamura is supported by a Grant-in-Aid for Scientific Research of JSPS. G. Nishimura is supported by a Grand-in-Aid for Scientific Research. Y. Jiang is supported by the National Natural Science Foundation of China. J. Liu is supported by NSFC. M. Machida is supported by a Grant-in-Aid for Scientific Research of JSPS. He also acknowledges the support by HUSM Grant-in-Aid.

Disclosures. The authors declare no conflicts of interest.

REFERENCES

- V. Ntziachristos, C. Bremer, and R. Weissleder, "Fluorescence imaging with near-infrared light: new technological advances that enable *in vivo* molecular imaging," *Eur. Radiol.* **13**, 195–208 (2003).
- V. Ntziachristos, J. Ripoll, L. V. Wang, and R. Weissleder, "Looking and listening to light: the evolution of whole-body photonic imaging," *Nat. Biotechnol.* **23**, 313–320 (2005).
- J.-C. Baritaux, K. Hassler, and M. Unser, "An efficient numerical method for general L_p regularization in fluorescence molecular tomography," *IEEE Trans. Med. Imag.* **29**, 1075–1087 (2010).
- D. Han, J. Tian, S. Zhu, J. Feng, C. Qin, B. Zhang, and X. Yang, "A fast reconstruction algorithm for fluorescence molecular tomography with sparsity regularization," *Opt. Express* **18**, 8630–8646 (2010).
- D. Han, X. Yang, K. Liu, C. Qin, B. Zhang, X. Ma, and J. Tian, "Efficient reconstruction method for L_1 regularization in fluorescence molecular tomography," *Appl. Opt.* **49**, 6930–6937 (2010).
- P. Mohajerani, A. A. Eftekhar, J. Huang, and A. Adibi, "Optimal sparse solution for fluorescent diffuse optical tomography: theory and phantom experimental results," *Appl. Opt.* **46**, 1679–1685 (2007).
- A. Behrooz, H.-M. Zhou, A. A. Eftekhar, and A. Adibi, "Total variation regularization for 3D reconstruction in fluorescence tomography: experimental phantom studies," *Appl. Opt.* **51**, 8216–8227 (2012).
- J. F. P.-J. Abascal, J. Chamorro-Servent, J. Aguirre, S. Arridge, T. Correia, J. Ripoll, J. J. Vaquero, and M. Desco, "Fluorescence diffuse optical tomography using the split Bregman method," *Med. Phys.* **38**, 6275–6284 (2011).
- V. Ntziachristos and R. Weissleder, "Experimental three-dimensional fluorescence reconstruction of diffuse media by use of a normalized Born approximation," *Opt. Lett.* **26**, 893–895 (2001).
- A. Koenig, L. Hervé, V. Josserand, M. Berger, J. Boutet, A. Da Silva, J.-M. Dinten, P. Peltié, J.-L. Coll, and P. Rizo, "In vivo mice lung tumor follow-up with fluorescence diffuse optical tomography," *J. Biomed. Opt.* **13**, 011008 (2008).
- V. Ntziachristos, C. H. Tung, C. Bremer, and R. Weissleder, "Fluorescence molecular tomography resolves protease activity *in vivo*," *Nat. Med.* **8**, 757–761 (2002).
- A. Corlu, R. Choe, T. Durduran, M. A. Rosen, M. Schweiger, S. R. Arridge, M. D. Schnall, and A. G. Yodh, "Three-dimensional *in vivo* fluorescence diffuse optical tomography of breast cancer in humans," *Opt. Express* **15**, 6696–6716 (2007).
- S. J. Erickson, S. L. Martinez, J. DeCerce, A. Romero, L. Caldera, and A. Godavarty, "Three-dimensional fluorescence tomography of human breast tissues *in vivo* using a hand-held optical imager," *Phys. Med. Biol.* **58**, 1563–1579 (2013).
- S. van de Ven, A. Wiethoff, T. Nielsen, B. Brendel, M. van der Voort, R. Nachabe, M. Van der Mark, M. Van Beek, L. Bakker, L. Fels, S. Elias, P. Luijten, and W. Mali, "A novel fluorescent imaging agent for diffuse optical tomography of the breast: first clinical experience in patients," *Mol. Imag. Biol.* **12**, 343–348 (2010).
- L. Hervé, A. Koenig, A. Da Silva, M. Berger, J. Boutet, J. M. Dinten, P. Peltié, and P. Rizo, "Noncontact fluorescence diffuse optical tomography of heterogeneous media," *Appl. Opt.* **46**, 4896–4906 (2007).
- V. Ntziachristos and R. Weissleder, "Charge-coupled-device based scanner for tomography of fluorescent near-infrared probes in turbid media," *Med. Phys.* **29**, 803–809 (2002).
- F. Stuker, J. Ripoll, and M. Rudin, "Fluorescence molecular tomography: principles and potential for pharmaceutical research," *Pharmaceutics* **3**, 229–274 (2011).
- C. Li, G. S. Mitchell, J. Dutta, S. Ahn, R. M. Leahy, and S. R. Cherry, "A three-dimensional multispectral fluorescence optical tomography imaging system for small animals based on a conical mirror design," *Opt. Express* **17**, 7571–7585 (2009).
- F. Gao, H. Zhao, L. Zhang, Y. Tanikawa, A. Marjono, and Y. Yamada, "A self-normalized, full time-resolved method for fluorescence diffuse optical tomography," *Opt. Express* **16**, 13104–13121 (2008).
- N. Ducros, C. D'Andrea, A. Bassi, and F. Peyrin, "Fluorescence diffuse optical tomography: time-resolved versus continuous-wave in the reflectance configuration," *IRBM* **32**, 243–250 (2011).
- G. Y. Panasyuk, Z.-M. Wang, J. C. Schotland, and V. A. Markel, "Fluorescent optical tomography with large data sets," *Opt. Lett.* **33**, 1744–1746 (2008).
- M. Mozumder, T. Tarvainen, S. Arridge, J. P. Kaipio, C. D'Andrea, and V. Kolehmainen, "Approximate marginalization of absorption and scattering in fluorescence diffuse optical tomography," *Inverse Probl. Imaging* **10**, 227–246 (2016).
- S. R. Arridge, "Optical tomography in medical imaging," *Inverse Probl.* **15**, R41–R93 (1999).
- K. Levenberg, "A method for the solution of certain non-linear problems in least squares," *Quart. Appl. Math.* **2**, 164–168 (1944).
- D. W. Marquardt, "An algorithm for least-squares estimation of nonlinear parameters," *J. Soc. Ind. Appl. Math.* **11**, 431–441 (1963).
- T. Goldstein and S. Osher, "The split Bregman method for L_1 -regularized problems," *SIAM J. Imaging Sci.* **2**, 323–343 (2009).
- J. F. Cai, S. Osher, and Z. Shen, "Split Bregman methods and frame based image restoration," *SIAM J. Multiscale Model. Simul.* **8**, 337–369 (2009).
- A. Marjono, A. Yano, S. Okawa, F. Gao, and Y. Yamada, "Total light approach of time-domain fluorescence diffuse optical tomography," *Opt. Express* **16**, 15268–15285 (2008).
- S. Okawa, A. Yano, K. Uchida, Y. Mitsui, M. Yoshida, M. Takekoshi, A. Marjono, F. Gao, Y. Hoshi, I. Kida, K. Masamoto, and Y. Yamada, "Phantom and mouse experiments of time-domain fluorescence tomography using total light approach," *Biomed. Opt. Express* **4**, 635–651 (2013).
- A. Ishimaru, *Wave Propagation and Scattering in Random Media* (Academic, 1978), Vol. 1.
- H. S. Carslaw and J. C. Jaeger, *Conduction of Heat in Solids* (Oxford University, 1959).
- K. Yosida and S. Ito, *Functional Analysis and Differential Equations* (Iwanami, 1976).
- A. H. Hielscher, S. L. Jacques, L. Wang, and F. K. Tittel, "The influence of boundary conditions on the accuracy of diffusion theory in time-resolved reflectance spectroscopy of biological tissues," *Phys. Med. Biol.* **40**, 1957–1975 (1995).
- M. Machida and G. Nakamura, "Born series for the photon diffusion equation perturbing the Robin boundary condition, to appear in *J. Math. Phys.*
- R. Fletcher, "A modified Marquardt subroutine for nonlinear least squares," Technical Report AERE-R 6799 (1971).
- J. J. Moré, "The Levenberg-Marquardt algorithm: implementation and theory," in *Numerical Analysis*, G. A. Watson, ed., Vol. **630** of Lecture Notes in Mathematics (Springer, 1977).

37. G. Nishimura, "Contrast improvement in indocyanine green fluorescence sensing in thick tissue using a time-gating method," *Biomed. Opt. Express* **10**, 1234–1249 (2019).
38. G. Nishimura, K. Awasthi, and D. Furukawa, "Fluorescence lifetime measurements in heterogeneous scattering medium," *J. Biomed. Opt.* **21**, 075013 (2016).
39. A. T. N. Kumar, J. Skoch, B. J. Bacska, D. A. Boas, and A. K. Dunn, "Fluorescence-lifetime-based tomography for turbid media," *Opt. Lett.* **30**, 3347–3349 (2005).
40. A. T. N. Kumar, S. B. Raymond, G. Boverman, D. A. Boas, and B. J. Bacska, "Time resolved fluorescence tomography of turbid media based on lifetime contrast," *Opt. Express* **14**, 12255–12270 (2006).
41. M. Hanke, "A regularizing Levenberg-Marquardt scheme, with applications to inverse groundwater filtration problems," *Inverse Probl.* **13**, 79–96 (1997).
42. Y. Jiang and G. Nakamura, "Convergence of Levenberg-Marquardt method for the inverse problem with an interior measurement," *J. Inverse Ill-Posed Probl.* **27**, 195–215 (2018).
43. W. L. Rice, S. Hou, and A. T. N. Kumar, "Resolution below the point spread function for diffuse optical imaging using fluorescence lifetime multiplexing," *Opt. Lett.* **38**, 2038–2040 (2013).
44. A. Zacharopoulos, M. Schweiger, V. Kolehmainen, and S. Arridge, "3D shape based reconstruction of experimental data in diffuse optical tomography," *Opt. Express* **17**, 18940–18956 (2009).
45. Q. Zhu, H. Dehghani, K. M. Tichauer, R. W. Holt, K. Vishwanath, F. Leblond, and B. W. Pogue, "A three-dimensional finite element model and image reconstruction algorithm for time-domain fluorescence imaging in highly scattering media," *Phys. Med. Biol.* **56**, 7419–7434 (2011).